A Theoretical Study of the Reaction between $CH_3S(OH)CH_3$ and O_2†

A. Gross,*,‡ I. Barnes,§ R. M. Sørensen,|| J. Kongsted,|| and K. V. Mikkelsen||,⊥

Meteorological Research Department, Danish Meteorological Institute (DMI), Lyngbyvej 100, DK-2100 Copenhagen Ø, Denmark, Fachbereich C—Physikalische Chemie, Bergische Universität Wuppertal, Gaussstrasse 20, 42097 Wuppertal, Germany, and Department of Chemistry, H. C. Ørsted Institute, University of Copenhagen, DK-2100 Copenhagen Ø, Denmark

Received: March 15, 2004; In Final Form: May 24, 2004

The geometries of $CH_3S(OH)CH_3$ (DMSOH) and DMSOH + O_2 have been investigated using ab initio and density functional theories. Reaction paths for the interaction between DMSOH and O_2 are established and potential energy surfaces/paths are calculated. On the basis of this information theoretical models for calculating the rate constants for the reactions DMSOH + O_2 → DMSO + HO_2 (where DMSO is used as abbreviation for $CH_3S(O)CH_3$) and DMSOH + O_2 + M → DMS(OH)(OO) + M (where DMS(OH)(OO) is used as abbreviation for $CH_3S(OH)(OO)CH_3$) have been developed and rate constants for these reactions have been estimated. For these two reactions the rate constants at 298 K are estimated to be 1.74×10^{-12} cm^3 molecule^{-1} s^{-1} and 8.63×10^{-34} cm^6 molecule^{-1} s^{-1}, respectively. After adjustment of the termolecular rate constants to typical atmospheric conditions, the atmospheric implications of DMSOH reaction with O_2 are discussed. The main conclusions from this work are: the most dominant channel for the outcome of the reaction DMSOH + O_2 is DMSO + HO_2. The reaction CH_3SOH + CH_3O_2 does not occur. On the other hand, this study shows that contributions to the total rate from the DMS(OH)(OO) reaction channel is possible. The sensitivity studies performed indicate that the DMS(OH)(OO) channel provides contribution to at most 50%. This is the first theoretical calculation of the rate constants involved in the DMSOH reactions with molecular oxygen.

1. Introduction

Dimethyl sulfide (CH_3SCH_3, DMS) is produced by marine phytoplankton. The emissions of DMS are estimated to account for approximately 25% of the total global gaseous sulfur released into the atmosphere.[1−6] The atmospheric oxidation of DMS is very complex. Furthermore, DMS can either be dissolved into aqueous-phase aerosols or oxidized to other sulfur gas-phase species which can contribute to aerosol formation. These gas-phase species are, e.g., SO_2, H_2SO_4, dimethyl sulfoxide ($CH_3S(O)CH_3$, DMSO), dimethyl sulfone ($CH_3S(O)_2CH_3$, $DMSO_2$), methanesulfinic acid ($CH_3S(O)OH$, MSIA) and methanesulfonic acid ($CH_3S(O)_2OH$, MSA).

Nearly 20 years ago Charlson et al.[7] put forward the hypothesis that emissions of DMS from the oceans can contribute to condensation nuclei formation and eventually to cloud condensation nuclei formation. The ramifications of this hypothesis are that DMS may have a significant regulatory influence on the Earth's radiation budget. This hypothesis has been investigated by several groups[8−12] using a variety of approaches which have resulted in disparate predictions of the possible role of DMS in climate regulation. One of the studies[12] has shown that understanding the fate of DMS in the gas-phase is of central importance if a realistic simulation of the contribution of DMS to condensation nuclei formation in the marine boundary layer is to be made.

The first highly detailed description of the photochemical fate of DMS in the gas-phase was given by Yin et al.[13,14] Other mechanisms have been proposed by Koga and Tanaka,[15] Capaldo and Pandis,[16] and Campolongo et al.[17] On the basis of these mechanisms and the most resent laboratory studies,[17−21] a gas-phase DMS mechanism has been developed for application to chamber experiments and atmospheric modeling within the EU Fifth Framework Program Project EL CID.[22]

Under low NO_x conditions, which is the case for the remote marine boundary layer, the most significant loss process for DMS is its reaction with OH, and this is currently believed to be the most important route for DMS during the daytime.[24] This reaction has been intensively studied experimentally[24−39] and theoretically.[40−44] From these studies, it has been established that this reaction proceeds via two reaction channels: a hydrogen atom abstraction by OH from one of the DMS methyl groups

$$CH_3SCH_3 + OH \rightarrow CH_3SCH_2 + H_2O \qquad (1)$$

(this reaction is O_2 independent), and a reaction corresponding to the formation of the reversible adduct $CH_3S(OH)CH_3$ (DMSOH):

$$CH_3SCH_3 + OH + M \rightleftharpoons CH_3S(OH)CH_3 + M \qquad (2)$$

Rate constant data evaluations of these two reactions and recommendations have been made by the NASA Panel for Data Evaluation[45] and the IUPAC Subcommittee on Gas Kinetic Data Evaluation of Atmospheric Chemistry.[46]

In this paper, we investigate the chemical fate of DMSOH when it reacts with ground-state $O_2(^3\Sigma_g)$. Hynes et al.[33] observed that in the presence of O_2 the loss of OH in the presence of DMS increases. This was explained by a reaction between DMSOH and O_2:

† Part of the "Gert D. Billing Memorial Issue".

* To whom correspondence should to addressed. E-mail: agr@dmi.dk.
‡ Danish Meteorological Institute (DMI).
§ Bergische Universität Wuppertal. E-mail: barnes@uni-wuppertal.de.
|| University of Copenhagen.
⊥ E-mail: kmi@theory.ki.ku.dk.

10.1021/jp048852z CCC: $27.50
Published on Web 07/21/2004

$$CH_3S(OH)CH_3 + O_2(^3\Sigma_g) \rightarrow \text{products} \quad (3)$$

In the absence of O_2 the adduct decomposition is rapid and only reaction 1 is observed. However, in the presence of O_2 the adduct reacts with O_2 to form products and the rate is dependent on the O_2 concentration. Under atmospheric conditions at 298 K, reaction 1 is the major channel; however, with decreasing temperature, reaction 2 and consequently reaction 3 become increasingly more important. Neither experimental nor theoretical investigations of reaction 3 have been performed. However, Hynes et al.[33,38] and Barone et al.[24] have studied the isotopic analogue of the following reaction:

$$CD_3S(OH)CD_3 + O_2(^3\Sigma_g) \rightarrow \text{products} \quad (4)$$

Hynes et al.[33] estimated the rate constant to be $(4.1 \pm 2.2) \times 10^{-12}$ cm^3 molecule^{-1} s^{-1} at a pressure of 700 Torr and temperature of 261 K, Hynes et al.[38] estimated the rate constant to be $(0.8 \pm 0.3) \times 10^{-12}$ cm^3 molecule^{-1} s^{-1} at a pressure of 110 Torr and temperatures of 250 and 258 K. Barone et al.[24] estimated the rate constant to be $(1.00 \pm 0.33) \times 10^{-12}$ cm^3 molecule^{-1} s^{-1} independent of pressure in the range 30−200 Torr of N_2 and temperature in the range 222−258 K.

Product channels of reaction 3 (and reaction 4) which are thermodynamically possible are[47]

$$CH_3S(OH)CH_3 + O_2 \begin{cases} \rightarrow CH_3S(O)CH_3 + HO_2 & \text{(a)} \\ \rightarrow CH_3S(OH)(OO)CH_3 & \text{(b)} \\ \rightarrow CH_3SOH + CH_3O_2 & \text{(c)} \\ \rightarrow CH_3S(O)_2CH_3 + OH & \text{(d)} \\ \rightarrow CH_3S(OH)(OO) + CH_3 & \text{(e)} \end{cases} \quad (5)$$

However, further reactions of the DMS(OH)(OO) complex could also lead to some of the products. For example, $CH_3S(OH)(OO)$ could be formed from a methyl radical expulsion from $CH_3S(OH)(OO)CH_3$ (DMS(OH)(OO)):

$$CH_3S(OH)(OO)CH_3 + M \rightarrow CH_3S(OH)(OO) + CH_3 + M \quad (6)$$

In a recent photoreactor product study, based on the variation of the product yield with reaction conditions, evidence has been presented that the major route for $DMSO_2$ formation in the OH initiated oxidation of DMS at atmospheric pressure under high NO_x concentrations is via reaction of the DMS(OH)(OO) radical with NO and subsequent reaction of $CH_3S(OH)(O)CH_3$ (DMS(OH)(O)) with O_2[47]:

$$CH_3S(OH)(OO)CH_3 + NO \rightarrow CH_3S(OH)(O)CH_3 + NO_2 \quad (7)$$

and

$$CH_3S(OH)(O)CH_3 + O_2 \rightarrow CH_3S(O)_2CH_3 + HO_2 \quad (8)$$

Under conditions of low NO_x concentrations significantly less $DMSO_2$ formation was observed and its formation was attributed to the self-reaction of DMS(OH)(OO) and/or its reaction with other peroxy radicals, e.g.

$$CH_3S(OH)(OO)CH_3 + CH_3S(OH)(OO)CH_3 \rightarrow 2\,CH_3S(OH)(O)CH_3 + O_2 \quad (9)$$

followed by reaction 8. Reaction of OH with DMSO is also a possible contributor to $DMSO_2$ formation, i.e.

$$CH_3S(O)CH_3 + OH + M \rightarrow CH_3S(OH)(O)CH_3 + M \quad (10)$$

again followed by reaction 8, but this was considered to be of minor importance in the study.

Figure 1 shows a schematic outline of the addition pathway in the reaction of OH with DMS which is based upon the results of the EL CID project[22] and recent literature data.[17−21] In Figure 1 only three reaction channels of the reaction of the DMSOH adduct with O_2 are included (reactions 5a, 5b, and 5c). Pathway 5d has been excluded because the experimental evidence suggests that $DMSO_2$ is produced via further reactions of DMS(OH)(OO) and not via decomposition of the radical. On the basis of the observed products pathway 5d is also deemed to be unimportant.[22] However, many uncertainties still exist with regard to the mechanism illustrated in Figure 1; these uncertainties are related to both the reaction pathways and the rate constants.[22,23,47]

The purpose of this study is to understand how DMSOH interacts with $O_2(^3\Sigma_g)$. As proved experimentally and illustrated in Figure 1, it is one of the fundamental reactions in the addition route of the reaction of OH with DMS. A detailed study of the interaction between DMSOH and $O_2(^3\Sigma_g)$ has therefore been carried out involving ab initio methods and density functional theory (DFT) for geometry optimizations, potential energy surface (PES) calculations, determination of reaction mechanisms, and rate constant calculations. This is the first investigation of the reaction between DMSOH and molecular oxygen where theoretical calculations have been performed for determining the relevant rate constants.

The paper mainly focuses on reactions 5a and 5b. We present optimized geometries of DMSOH and DMS(OH)(OO). The results from these investigations are presented in sections 2.1 and 2.2. On the basis of these optimized geometries, reaction mechanisms for reactions 5a and 5b are proposed and in section 2.2 used to calculate constrained PESs (CPESs).

On the basis of the proposed mechanisms for reactions 5a and 5b and the calculated CPES, theoretical models have been established and rate constants have been calculated (section 3). From these theoretically calculated rates and the experimentally determined rate constant[24,38] of the overall reaction DMSOH + O_2 → products the rate constant for reaction 5c has been evaluated; see section 4.

Thus, the present study provides important information on the fate of the DMSOH adduct in the addition channel of DMS + OH and provides a basis for discussion on the branching ratio of three of the channels (a, b, and c) of reaction 5. This and the other results obtained are discussed in section 4.

2. Calculations Using Second-Order Møller−Plesset Perturbation and Density Functional Theories

To understand the addition pathway of DMS + OH various calculations using the ab initio method second-order Møller−Plesset (MP2) perturbation theory[48] and DFT[48] have been performed on different molecules involved in the addition pathway reaction mechanism. For this purpose, Gaussian 98[49] has been used. In this section, we present the results obtained for DMSOH and various DMS−(OH)−(OO) complexes, and reaction mechanisms are proposed. The determinations of vibrational frequencies of the structures obtained from the geometry optimizations indicate that all the relevant molecules are in local minima on the PES (an exception is the identified transition state).

Turecek[42] along with Wang and Zhang[44] have also studied the DMSOH radical using ab initio theory and DFT. The results from their work are also discussed.

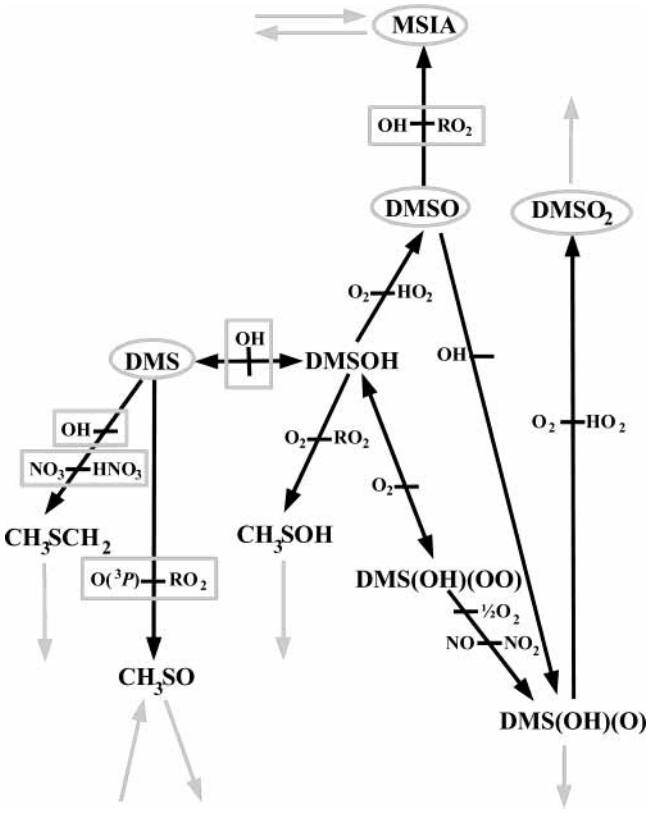

Figure 1. Schematic representation of the initial steps in the OH radical initiated photooxidation of DMS. Gas-phase species encased in a gray ellipse are in equilibrium with liquid-phase aerosols. For reactions encased in a gray box the rate constant has been determined in laboratory experiments. The gray arrows symbolize the existence of other possible reaction routes (sources or sinks) for the sulfur gas-phase compounds presented in the figure. $RO_2 = CH_3O_2$.

2.1. DMSOH: Calculations, Results, and Discussion. Eleven different calculations of DMSOH have been performed. We used DFT using Becke's three-parameter hybrid functional together with Lee, Yang, and Parr's correlation functional (B3LYP)[50,51] and DFT combined with the Perdew/Wang gradient corrected correlation and exchange functional (PW91PW91)[52,53] as well as MP2[54] with different basis sets for geometry optimizations of DMSOH. The use of PW91 functionals for both correlation and exchange is recommended by Perdew et al.[52] since in this case the errors in exchange and correlation contributions tend to cancel. The employed basis sets are 6-311G**,[55] cc-pVDZ, cc-pVTZ, aug-cc-pVDZ and aug-cc-pVTZ.[56−58] Optimizations and frequency calculations were carried out for each of the 11 calculations. The geometries obtained from these calculations are illustrated in Figure 2, and the distances (as indicated in Figure 2) between the S and O atoms in the optimized geometries are listed in Table 1.

Figure 2 shows that for all the geometries the two methyl groups are in an eclipsed position to each other. The geometries obtained using DFT and the 6-311G** basis set are different from the result obtained using the same basis set and MP2 theory. The differences are illustrated in Figure 2, parts a, d, and g. We observe that in the MP2 calculation the H atom is closest to the S atom whereas in the DFT calculations it is closest to the O atom. Such a local minimum is not found for the B3LYP/6-311G** calculation. Because of this discrepancy the same calculations were performed with Dunnings correlation consistent basis sets: cc-pVDZ, aug-cc-pVDZ, cc-pVTZ, and aug-cc-pVTZ. The MP2/cc-pVDZ calculation gave the same geometry of DMSOH as the MP2/6-311G** calculation, whereas the MP2 calculations with aug-cc-pVDZ, cc-pVTZ, and aug-cc-pVTZ basis sets resulted in the same geometry as B3LYP/6-311G**. This indicates that DFT calculations with a 6-311G** basis set provide a reliable determination of the structures. Thereby, we avoid the significantly more expensive MP2 calculations of geometries and vibrational frequencies.

The geometries of DMSOH identified in this work, see Figure 3, are in agreement with the geometries obtained by Turecek;[42] however, there is a contradiction with the results from Wang and Zhang,[44] since their optimized configuration using the MP2/cc-pVTZ method corresponds to our MP2/cc-pVDZ and MP2/6-311G** structures.

As seen from Table 1 going from B3LYP and PW91PW91 to MP2, and if the basis set is increased, the bond length of S−O in DMSOH decreases (except for MP2/cc-pVDZ and MP2/6-311G**) as expected. As observed in Wang and Zhang[44] and Turecek[42] a significant part of the stabilization energy of DMSOH is related to the attractive dipole−dipole interaction between DMS and OH.

For an accurate description of the weakly bound adduct, DMSOH, the results here indicate that reasonably large basis sets are required in order to recover a large fraction of the correlation energy. Considering the amount of detail with which the systems are examined in this paper, it was not possible to use the best and most accurate electronic structure methods and basis sets. From the calculations performed here and a comparison with the results obtained by Wang and Zang[44] and Turecek[42] it is evident that the most stable DMSOH complexes are those in Figure 2, parts a−f, h, i, and k, and these DMSOH complexes are almost identical. Therefore, we have utilized the method PW91PW91/6-311G** for further examination of the DMS−(OH)−(OO) system.

2.2. DMS−(OH)−(OO): Calculations, Results and Discussion. As described in the introduction of this paper, the reaction between DMSOH and O_2 has three possible product channels. We have performed MP2/6-311G** and PW91PW91/6-311G** calculations on the DMS−(OH)−(OO) complex in order to understand the reaction mechanism of these reaction channels. Our investigation resulted in the identification of the following:

- two van der Waals complexes, Figure 3a,b.
- one transition state, Figure 3c.
- four stable complexes of DMS(OH)(OO) where the OH radical and the O_2 molecule are directly bonded to the S atom, Figure 3d-g.

For all these identified compounds the results from the MP2/6-311G** and PW91PW91/6-311G** calculations agree reasonably well. Some of these complexes were also obtained in the study by Wang and Zhang[44] which will be discussed below.

2.2.1. Identification of Two van der Waals Complexes and One Transition State. The MP2/6-311G** and PW91PW91/6-311G** calculations of the DMS−(OH)−(OO) complex gave rise to two van der Waals complexes, the structures of which are shown in Figure 3, parts a and b. Wang and Zhang[44] only reported the van der Waals complex shown in Figure 3a. On the basis of this identification we predicted that a transition state between the two van der Waals complexes exists, however, it was not possible to use Gaussian 98 to search for the transition state. Therefore, a number of PW91PW91/6-311G** calculations, with geometry optimization of the van der Waals complex, were performed at different r_{SOH-OO} (the distance between SO and HOO in the complex) and r_{SOH-OO} (the distance between SOH and OO in the complex) distances. The values of r_{SOH-OO}

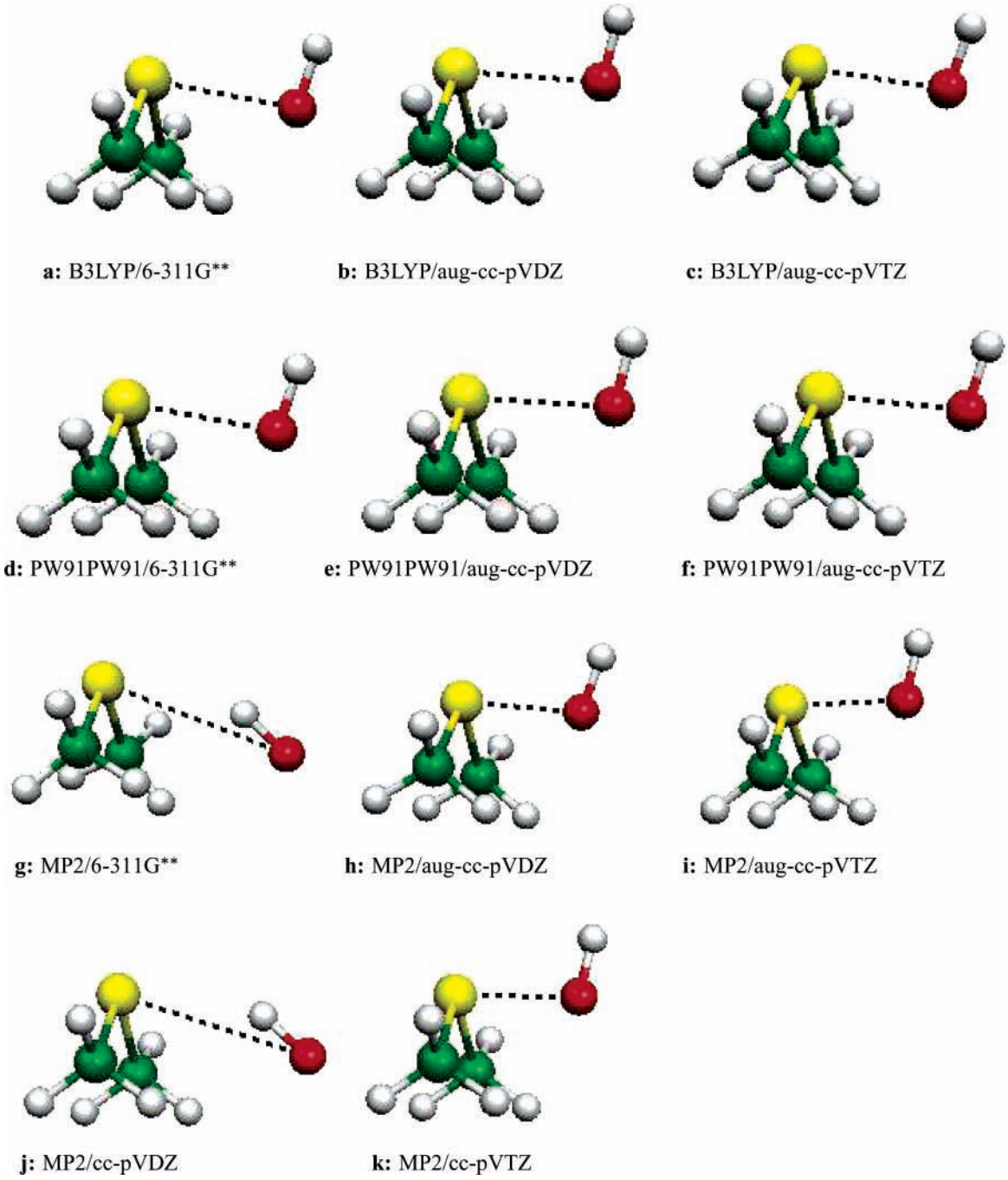

Figure 2. Optimized geometries of DMSOH using B3LYP, PW91PW91 and MP2, and five different basis sets. Yellow: the sulfur atom. Green: the carbon atoms. Red: the oxygen atom. White: the hydrogen atoms.

TABLE 1: Distance between the Sulfur and Oxygen Atom in the Optimized Geometries of DMSOH for the Five ab Initio and Six DFT Calculations[a]

method/basis set	6−311g**	cc-pVDZ	cc-pVTZ	aug-cc-pVDZ	aug-cc-pVTZ
B3LYP	2.372			2.334	2.312
PW91PW91	2.312			2.286	2.261
MP2	3.292	3.311	2.038	2.267	2.023

[a] Results are in Å.

and r_{SOH-OO} were varied from 0.78 to 1.88 Å and from 0.83 to 2.48 Å, respectively, with a spacing of 0.05 Å. A plot of the potential energy from these calculations as a function of r_{SOH-OO} and r_{SOH-OO} is presented in Figure 4 (ground-state CPES). A frequency analysis of these calculations showed that a transition state was located at $r_{SOH-OO} = 0.980$ Å and $r_{SOH-OO} = 1.570$ Å; see Table 2. The located transition state is plotted in Figure 3c.

Comparing Figure 4 with Figure 3c, the relative energies, r_{SOH-OO} and r_{SOH-OO} in the van der Waals complexes and the transition state, we observe that the transition state is located in the entrance channel of the CPES and that the van der Waals complex **3a** has to overcome a barrier of only 0.140 eV in order to break the O−H bond and form the peroxy radical HO_2. The product channel has a potential energy which is 0.662 eV lower than the reactant channel.

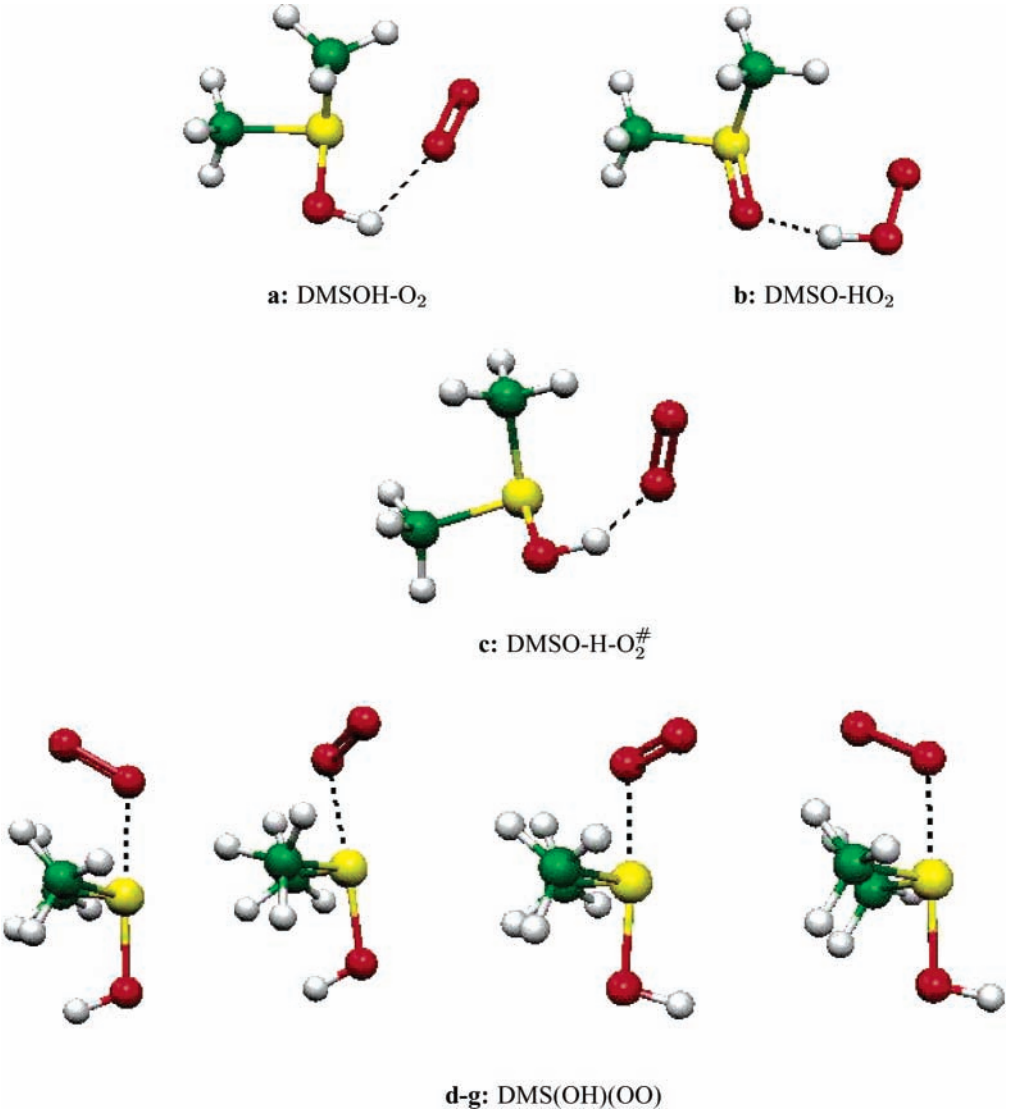

Figure 3. Optimized geometries of the two van der Waals complexes (MP2/6-311G**) (a and b), the transition state that exists between the two van der Waals (PW91PW91/6-311G**) (c), and the four different DMS(OH)(OO) complexes (MP2/6-311G**) (d−g). Yellow: the sulfur atom. Green: the carbon atoms. Red: the oxygen atoms. White: the hydrogen atoms.

The formation of van der Waals complexes occurs without potential energy barriers. On the basis of the CPES in Figure 4 it is therefore natural to assume that reaction 5a proceeds via the following three-step mechanism. First, an equilibrium between DMSOH + O_2 and the van der Waals complex **3a** is reached relatively fast:

$$\mathrm{DMSOH} + \mathrm{O_2} \underset{k_{5a}^{eq}}{\overset{k_{-5a}^{eq}}{\rightleftharpoons}} \mathrm{DMSOH{-}O_2} \qquad (11)$$

DMSO−HO_2 is then formed from DMSOH−O_2 by first forming the activated complex (transition state, DMSO−H−$O_2^{\#}$). Using transition state theory (TST), the following reaction sequence can be assumed:

$$\mathrm{DMSOH{-}O_2} \rightleftharpoons \mathrm{DMSO{-}H\text{-}O_2^{\#}} \rightarrow \mathrm{DMSO{-}HO_2} \qquad (12)$$

Finally, the product van der Waals complex equilibrates with DMSO + HO_2:

$$\mathrm{DMSO{-}HO_2} \underset{k_{5a}^{eq}}{\overset{k_{-5a}^{eq}}{\rightleftharpoons}} \mathrm{DMSO} + \mathrm{HO_2} \qquad (13)$$

This three step mechanism is in contradiction with the mechanism proposed by Wang and Zhang.[44] They proposed the following two channel mechanism for DMSO formation:

$$\mathrm{DMSOH} + \mathrm{O_2} \rightleftharpoons \mathrm{DMS(OH)(OO)} \begin{cases} \rightarrow \mathrm{DMSO} + \mathrm{HO_2} \\ \overset{\mathrm{O_2}}{\underset{\mathrm{HO_2}}{\downarrow}} \mathrm{DMS(O)(OO)} \rightarrow \mathrm{DMSO} + \mathrm{O_2} \end{cases} \qquad (14)$$

However, our three step mechanism is in agreement with the results from the study by Yin et al.[13,14] and Turnipseed et al.[59] In section 3, we present how the rate constant can be calculated from this three-step mechanism.

2.2.2. The DMS(OH)(OO) Complexes. The PW91PW91/6-311G** and MP2/6-311G** calculations confirm the existence of four stable DMS(OH)(OO) complexes, and all these complexes are in local minima. These four complexes are illustrated in Figure 3d−g. The complexes correspond to different rotations of the HO and O_2 groups around the S atom. From the four illustrations it can be seen that (1) when O_2 is directly above the methyl groups, the two methyl groups are in an eclipsed position relative to one another, and (2) when O_2 is

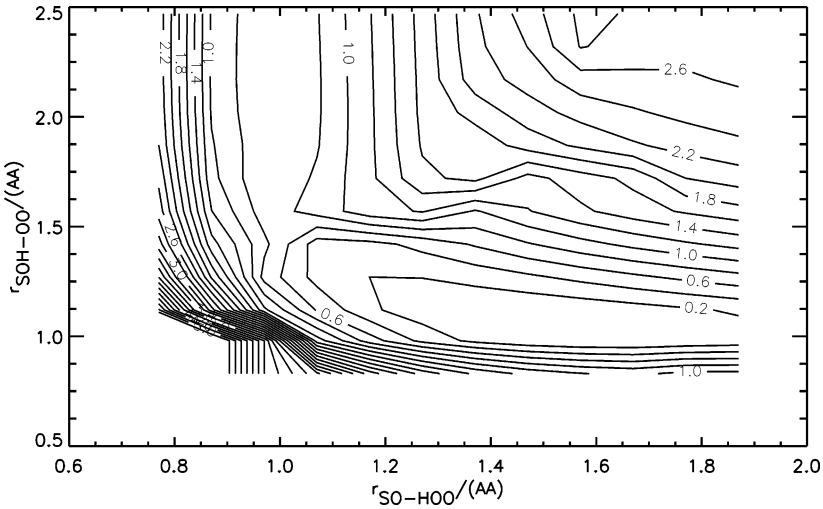

Figure 4. Contour map of the ground state of DMSO−H−OO. The PES is obtained by performing geometry optimization of the van der Waals complex at different r_{SO-HOO} (the distance between SO and HOO in the complex) and r_{SO-HOO} (the distance between SOH and OO in the complex) distances. The values of r_{SO-HOO} and r_{SO-HOO} were varied from 0.78 to 1.88 Å and from 0.83 to 2.48 Å, respectively, with a spacing of 0.05 and 0.05 Å. Geometry optimization calculation: PW91PW91/6-311G**. The contour increment is 0.2 eV.

TABLE 2: Distances and Relative Energies (ΔE_a) and ΔE_a + ΔZPE of the Two DMS−(OH)−(OO) van der Waals Complexes, the Transition State, and the Four DMS(OH)(OO) Complexes[a]

	ΔE_a, eV	ΔE_a + ΔZPE, eV	r_{SO-HOO}, Å	r_{SO-HOO}, Å
		MP2/6-311G** Calculation		
DMSOH−O_2	0.000	0.000	0.970	1.975
DMSO−HO_2	−1.137	−1.114	1.596	1.001
		PW91PW91/6-311G** Calculation		
DMSOH−O_2	0.000	0.000	0.978	2.169
TST	0.163	0.140	0.980	1.570
DMSO−HO_2	−0.654	−0.662	1.550	1.034
	ΔE_a, eV	ΔE_a + ΔZPE, eV	r_{S-OH}, Å	r_{S-O_2}, Å
		MP2/6-311G** Calculation		
DMS(OH)(OO) a	0.000	0.000	1.745	2.076
DMS(OH)(OO) b	−0.0730	−0.0790	1.756	2.000
DMS(OH)(OO) c	−0.214	−0.218	1.778	1.994
DMS(OH)(OO) d	−0.245	−0.246	1.772	2.068
		PW91PW91/6-311G** Calculation		
DMS(OH)(OO) a	0.000	0.000	1.821	2.186
DMS(OH)(OO) b	−0.0250	−0.022	1.838	2.126
DMS(OH)(OO) c	−0.140	−0.152	1.859	2.084
DMS(OH)(OO) d	−0.154	−0.161	1.853	2.284

[a] For the van der Waals complexes the energies are calculated relative to the DMSOH−O_2. For the DMS(OH)(OO) complex structures, the energies are calculated relative to structure a. ΔZPE is the difference between the zero point vibrational energies. r_{SO-HOO}, r_{SOH-OO}, r_{S-OH}, and r_{S-O_2} are the distances between SOH and OO in the van der Waals complexes and the distances between S−OH and S−OO in the DMS(OH)(OO) complex, respectively.

turned away from the methyl groups, the two methyl groups are in a staggered position relative to each other, due to the influence from the O_2 electron-cloud on the methyl groups. Table 2 shows that complexes **a** and **b** and complexes **c** and **d** have very similar energies, and the structures of **c** and **d** have the lowest energies. If O_2 is removed from the two most stable complexes a DMSOH radical with a geometry close to the most stable DMSOH radical is identified; compare with section 2.1. Therefore, we propose that DMS(OH)(OO) is formed as follows:

$$\text{DMSOH} + \text{O}_2 \begin{cases} \rightarrow \text{DMS(OH)(OO)} & \text{(structure } \mathbf{c}\text{)} \\ \rightarrow \text{DMS(OH)(OO)} & \text{(structure } \mathbf{d}\text{)} \end{cases} \quad (15)$$

Since no bond breaking is involved in the formation of DMS(OH)(OO), it is reasonable that the formation of DMS(OH)(OO) is a reaction without a potential barrier. This was confirmed by an estimation of the potential energy reaction path for O_2 approaching the S atom in DMSOH. This calculation showed that the distance between the center of the masses of DMSOH and O_2 had a potential energy minimum at 2.819 Å, a dissociation energy of 0.7325 eV, and no potential barrier.

The formation of a stable DMS(OH)(OO) complex can be described as a termolecular recombination reaction.[60−67] The overall termolecular reaction is divided into a mechanism involving two bimolecular steps. First, in an equilibrium between DMSOH + O_2 a highly ro-vibrationally excited DMS(OH)-(OO)* is reached relatively fast:

$$\text{DMSOH} + \text{O}_2 \underset{k_{5b}^{eq}}{\overset{k_{5b}^{eq}}{\rightleftharpoons}} \text{DMS(OH)(OO)*} \quad (16)$$

This quasi-bound molecule is then deactivated to a stable DMS(OH)(OO) complex by a third inert body (in the atmosphere this is typically O_2 or N_2):

$$\text{DMS(OH)(OO)*} + \text{M} \xrightarrow[k_{5b}']{} \text{DMS(OH)(OO)} + \text{M} \quad (17)$$

This two-step mechanism belongs to the class of an energy-transfer mechanism. A Chaperon (exchange) mechanism has also been proposed for this kind of reaction; however, if M = O_2, then the energy-transfer and Chaperon mechanism will be identical. On the other hand, if M = N_2, it is safe to assume that tight van der Waals complexes between N_2 and DMSOH are not formed. Hence, only the energy transfer mechanism is proposed to be important for formation of stable DMS(OH)(OO). A model to calculate rate constants for termolecular reactions will be described in section 3.

3. Theoretically Calculated Rate Constants

Reactions without a potential energy barrier (loose transition states) have quite different dynamics compared to reactions with potential energy barriers (tight transition states). Clearly, this is related to the nature of the PES and it can be explained as follows. For the PES with a barrier the reaction occurs in a region of the PES that is quite different from both reactants and products, i.e., at the saddle point. For loose transition states the reaction occurs at relatively large separations of two dissociating or recombining fragments, i.e., the PES is "product-like". Furthermore, for recombination reactions without a potential energy barrier a third body is needed in order to form a stable molecule. In the following the theoretical methods used for calculating the rate constants for reactions 5a and 5b will be described.

3.1. Reaction 5a. Reaction 5a occurs by the initial formation of a van der Waals complex, e.g., a reaction without a potential barrier under the formation of a loose transition state. This is followed by a chemical reaction with a well-defined transition state as shown in Figure 4. The reaction product from the latter reaction is another van der Waals complex. Assuming reaction sequence 12 follows the TST, we have

$$\mathrm{DMSOH{-}O_2} \xrightarrow{k_5^{\#}} \mathrm{DMSO{-}HO_2} \tag{18}$$

Furthermore, we assume that equilibriums between DMSOH + O_2 and DMSOH$-O_2$, and DMSO$-HO_2$ and DMSO + HO_2 are reached relatively quickly, and therefore

$$\frac{\mathrm{d[DMSOH{-}O_2]}}{\mathrm{d}t} \approx 0$$

and

$$\frac{\mathrm{d[DMSO{-}HO_2]}}{\mathrm{d}t} \approx 0 \tag{19}$$

From these assumptions it is possible to derive the following equation for the overall rate constant, k_{5a}^{tot}:

$$k_{5a}^{tot} = \frac{k_{5a}^{eq} k_{5a}^{\#}}{k_{-5a}^{eq} + k_{5a}^{\#}} \approx \frac{k_{5a}^{eq}}{k_{-5a}^{eq}} k_{5a}^{\#} \tag{20}$$

presuming that the bond-breaking sequence of the reaction is the rate-determining step. Since a well-defined transition state for this reaction is found (see Figure 3c) TST is used for calculating the rate constant for reaction 18.

Consider

$$k(T,s) = \sigma g \frac{k_B T}{h} \frac{Q_{rot}(s) Q_{vib}(s)}{Q_{rot}^{DMSOH-O_2} Q_{vib}^{DMSOH-O_2} Q_t^{rel}} \exp(-V_0(s)/k_B T) \tag{21}$$

where σ is the symmetry factor counting the number of equivalent reaction paths, g is the combined electronic degeneracy factor of the reactant and the complex at point s of the reaction path, k_B is the Boltzmann constant, T is the temperature, h is Planck's constant, $Q_{rot}^{DMSOH-O_2}$ is the rotational partition function for the reactant, $Q_{vib}^{DMSOH-O_2}$ is the vibrational partition function for the reactant, Q_t^{rel} is the translational partition function per unit volume for the relative translational motion, $V_0(s)$ the difference between the potential and zero-point energies of the system at point s of the reaction path relative to the reactant, $Q_{rot}(s)$ is the rotational partition function for the system at point s of the reaction path, and $Q_{vib}(s)$ is the vibrational partition function for the system at point s of the reaction path. The TST rate constant is then given by

$$k^{\#}(T) = k(T, s = \#) \tag{22}$$

where # symbolizes the saddle point,[68] i.e., the transition state.

The equilibrium between DMSOH + O_2 and the van der Waals complex DMSOH$-O_2$ described in reaction 11 can also be obtained using statistical mechanics. From Gilbert and Smith[69] we get

$$\frac{k_{5a}^{eq}}{k_{-5a}^{eq}} = \sigma g \frac{k_B T}{h} \frac{Q_{rot}^{DMSOH-O_2} Q_{vib}^{DMSOH-O_2}}{Q_{rot}^{DMSOH} Q_{vib}^{DMSOH} Q_{rot}^{O_2} Q_{vib}^{O_2} Q_t^{rel}} \exp(-\Delta E_{5a}/k_B T) \tag{23}$$

where ΔE_{5a} is the difference in the zero-point energies between the reactants and product for the equilibrium described in eq 11. The term $Q_{rot}^{DMSOH-O_2}$ ($Q_{vib}^{DMSOH-O_2}$) is the rotational (vibrational) partition function for DMSOH$-O_2$, Q_{rot}^{DMSOH} (Q_{vib}^{DMSOH}) is the rotational (vibrational) partition function for DMSOH, and $Q_{rot}^{O_2}$ ($Q_{vib}^{O_2}$) is the rotational (vibrational) partition function for O_2.

The rate constants obtained using this theory for reaction 5a are plotted in Figure 5. For comparison the experimental measurements from Hynes et al.[33,38] and Barone et al.[24] are also plotted in Figure 5.

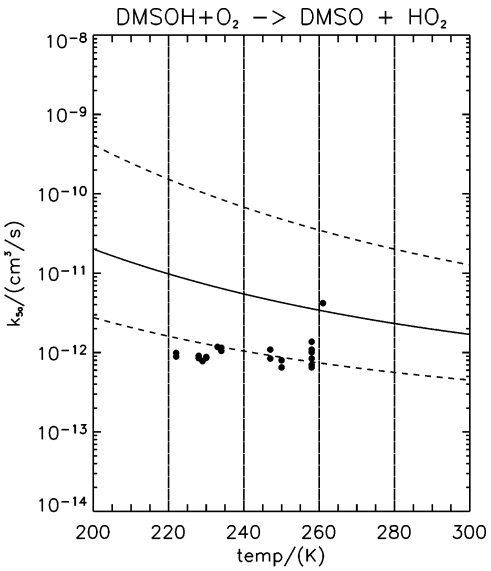

Figure 5. Calculated rate constants (solid line) and estimated errors (dashed lines) for reaction 5a as a function of temperature. The dots are the experimentally measured rate constants displayed in Table 6. The rate constants are estimated using the theoretical model described in section 3.1. The errors are estimated from the assumption that the relative energies displayed in Table 3 have a possible error of 10%.

3.2. Reaction 5b. To calculate the overall rate constant for reaction 5b

$$\mathrm{DMSOH} + \mathrm{O_2} + \mathrm{M} \xrightarrow{k_{5b}^{tot}} \mathrm{DMS(OH)(OO)} + \mathrm{M} \quad (24)$$

a steady-state treatment of [DMS(OH)(OO)*] is assumed. This gives

$$k_{5b}^{tot} = k'_{5b}\frac{k_{5b}^{eq}}{k_{-5b}^{eq}}\frac{k_{-5b}^{eq}}{k_{-5b}^{eq} + k'_{5b}[\mathrm{M}]} \approx k'_{5b}\frac{k_{5b}^{eq}}{k_{-5b}^{eq}} \quad (25)$$

where the limiting condition $k_{-5b}^{eq} \gg k'_{5b}[\mathrm{M}]$ is used.[66−70] Therefore, this approximation assumes that a thermal equilibrium between DMSOH + O_2 and DMS(OH)(OO) is reached very quickly and that the deactivation step is the rate-determining step.

Different approaches have been used to calculate the termolecular rate constants for different energy-transfer mechanisms ranging from full quasi-classical trajectory methods[66−70] to statistical[69] and empirical-adapted[69,71] methods. However, for large polyatomic molecules, full quasi-classical methods are not feasible since it is problematic to obtain sufficient information on the PES. Statistical methods can also be difficult to apply because a detailed and good description of the quasi-bound complex, to be deactivated, is necessary. In this paper we aim at describing the formation and deactivation of DMS(OH)(OO)*, however, in this study it has not been possible to obtain spectroscopic information on the highly energized molecule. Therefore, a new and simple semiempirical model has been developed in order to describe the formation of the stable structure of DMS(OH)(OO).

Because of missing information about the structure and spectroscopic data on DMS(OH)(OO)*, we assumed that DMS(OH)(OO)* is a spherical mass which is formed from a collision of two spherical masses O_2 and DMSOH (i.e., rotational and vibrational degrees of freedoms of the molecules are ignored). This approximation makes it possible to describe k_{5b}/k_{-5} as[62]

$$\frac{k_{5b}^{eq}}{k_{-5b}^{eq}} = \int_0^\infty \mathrm{d}(E_{kin}^{eq}/k_B T)\int_0^{b_{max}^{eq}} \mathrm{d}b\; E_{kin}^{eq}/k_B T \times \exp(-E_{kin}^{eq}/k_B T)\, z(E_{kin}^{eq}, \mathrm{b}^{eq})\, \tau(E_{kin}^{eq}) \quad (26)$$

where E_{kin}^{eq} is the relative kinetic energy between O_2 and DMSOH, b^{eq} is the impact parameter of the reaction, b_{max}^{eq} is the maximum impact parameter for which scattering can occur. The term $z(E_{kin}^{eq}, b)$ is the collision number between DMSOH and O_2 at E_{kin}^{eq} and b^{eq}, and $\tau(E_{kin}^{eq})$ is the average lifetime of DMS(OH)(OO)* at E_{kin}^{eq}.

We assume that the potential energy of the reaction path follows a Lennard-Jones potential and we obtain a simple analytical expression of eq 26:

$$\frac{k_{5b}^{eq}}{k_{-5b}^{eq}} = \frac{9}{2}{\sigma_{LJ}}^3\sqrt{2\pi\epsilon_{LJ}/k_B T} \quad (27)$$

where σ_{LJ} and ϵ_{LJ} are the Lennard-Jones parameters. We observe from eq 27 that only the dissociation energy and the equilibrium distance are necessary in order to calculate the equilibrium constant.

The deactivation of a quasi-bound molecule cannot be calculated realistically using the hard-sphere approximation. The hard-sphere approximation will overestimate k_{5b}^{tot}.[65−67] Even though there is no evidence that the deactivation of the quasi-bound molecule (the reaction probability) follows an exponential decay, we note that different theoretical studies have shown that to be the case.[66−69,71] Therefore, we propose the following model for the deactivation process.

Consider the following general energy-transfer reaction:

$$\mathrm{A} + \mathrm{B} \rightleftharpoons \mathrm{AB^*} \quad (28)$$

$$\mathrm{AB^*} + \mathrm{M} \rightarrow \mathrm{AB} + \mathrm{M} \quad (29)$$

First, we assume that the reaction probability, p_{deac}, for reaction 29 follows

$$p_{deac} = \begin{cases} 0 & \text{if } b^{deac} > b_{max}^{deac} \\ p'_{deac}(E_{AB^*}, E_M, {E_{kin}}^{AB^*-M}) & \text{else} \end{cases} \quad (30)$$

where E_{AB^*} is the energy of the quasi-bound molecule AB*, E_M is the energy of the third body M, and $E_{kin}^{AB^*-M}$ is the kinetic energy of the translational motion between M and AB*. Second, we assume that p' decays exponentially:

$$p'_{deac}(E_{A^*}, E_M, E_{kin}^{AB^*-M}) = \beta \exp\left(-\alpha\frac{E_{AB^*} + E_M + E_{kin}^{AB^*-M}}{\langle\Delta E_{trans}\rangle}\right) \quad (31)$$

where α and β are dimensionless parameters, and $\langle\Delta E_{trans}\rangle$ is the average energy transferred to M when it collides with AB*. We observe that p'_{deac} behaves physically correct since larger $\langle\Delta E_{trans}\rangle$ results in slower exponential decay of p'_{deac}. From this we derive the following ro-vibrational collision cross-section, $\sigma_{AB^*,M}^{v,j}$:

$$\sigma_{deac}^{v,j}(E_{AB^*}, E_M, E_{kin}^{AB^*-M}) = \pi\,(b_{max}^{deac})^2\beta \times \exp\left(-\alpha\frac{E_{A^*} + E_M + E_{kin}^{AB^*-M}}{\langle\Delta E_{trans}\rangle}\right) \quad (32)$$

where v and j are the ro-vibrational quantum numbers of M. The deactivation rate constant k'_{29} (which corresponds to k'_{5b} in reaction 5b) can then be obtained by weighting the cross-section with the ro-vibrational partition-function of M followed by averaging E_{AB^*}, E_M, $E_{kin}^{AB^*-M}$ with respect to the Boltzmann distribution and integration. This gives

$$k'_{5b} = \sqrt{\frac{8k_B T}{\pi\mu_{AB^*,M}}}\pi(b_{max}^{deac})^2\frac{\beta}{(k_B T\alpha/\langle\Delta E_{trans}\rangle)^3} \times \exp(-\alpha E_D/\langle\Delta E_{trans}\rangle) \quad (33)$$

where E_D is the dissociation energy of AB → A + B (for reaction 5b it is the dissociation energy for DMSOHOO → DMSOH + O_2). The term $\mu_{AB^*,M}$ is the reduced mass of the AB*,M system.

Before eq 33 can be used, the two dimensionless parameters α and β must be selected. We have set β equal to 0.5 for all the calculations of the termolecular rate constants presented in this paper, because when $E_{tot}^{AB} = E_{AB^*} + E_M + E_{kin}^{AB^*-M}$ is close to zero the energy of AB* will only be slightly larger than E_D and the energy of M will not be very high. It is more difficult to make an argument for a good choice of α. However, we propose to set $\alpha = (T/300\ \mathrm{K})^a$ where a is selected such that the temperature dependence of k_{5b}^{tot} is similar to other termolecular

TABLE 3: Relative Energies (ΔE_a) and $\Delta E_a + \Delta ZPE$ of Different Product Channels Shown in Figure 1 Relative to Reactant Channel DMSOH + O_2[a]

	PW91PW91/6-311G** calcd	
reaction	ΔE_a, eV	$\Delta E_a + \Delta ZPE$, eV
DMSOH + $O_2(^3\Sigma_u)$	0.0000	0.0000
DMSOH−O_2	−0.4169	−0.2907
DMS−H−O_2[#]	−0.2534	−0.1498
DMSO−HO_2	−1.0713	−0.9523
DMSO + HO_2	−0.2387	−0.1964
DMSOHOO a	−0.7075	−0.5824
DMSOHOO b	−0.7325	−0.6044
DMSOHOO c	−0.8475	−0.7344
DMSOHOO d	−0.8615	−0.7434
$CH_3SOH + CH_3O_2$	−0.6378	−0.5498

[a] ΔZPE is the difference between the zero point vibrational energies.

TABLE 4: Dissociation Energies (E_D), Equlibrium Distances for the Bonding in the Triatomic Molecule That Breaks, Lennard-Jones Parameters, and Average Energy Transfer Quantities of M (ΔE_{trans}) When It Collides with a Molecule[a]

$O + O_2 + M \rightarrow O_3\,M$

E_D of $^2P + X,^3\Sigma_g^-$	equilibrium distribution of O−O_2
1.13 eV	1.278 Å

$Cl + O_2 + M \rightarrow ClO_2 + M$

E_D of $^3P + X,^3\Sigma_g^-$	equilibrium distribution of Cl−O_2
2.56 eV	1.473 Å

Lennard-Jones Parameters

	$O_2(X,^3\Sigma_g^-)$	$N_2(X,^1\Sigma_g^+)$
ϵ/k_b	113.27 K	91.85 K
	3.654 Å	3.919 Å

Typical ΔE_{trans} Values

$O_2(X,^3\Sigma_g^-)$	$N_2(X,^1\Sigma_g^+)$
160 cm^{-1}	130 cm^{-1}

[a] The E_D values and equilibrium distances are taken from Herzberg,[72,73] Lennard-Jones parameters from Cuadros et al.,[74] and average energy transfer quantities from Hippler et al.[75]

reactions of the same type. If such information is not available we propose to use $\alpha = 1$. This choice of α is investigated below.

3.2.1. Test of the Model and Determination of Parameters. We want to apply this simple semiempirical model to calculate rate constants for the deactivation of DMS(OH)(OO)* with the most typical inert atmospheric molecules N_2 and O_2. However, this process has not been investigated before; we have therefore, if we use the newly developed model described above, neither theoretical nor experimental results to compare our results with. Thus, before we used the semiempirical model on reaction 5b a test has been conducted on two experimentally investigated termolecular reactions:

$$O(^3P) + O_2(X,^3\Sigma_g^-) + M \xrightarrow{k_{33}} O_3(\tilde{X},^1A_1) + M \quad (34)$$

and

$$Cl(^2P) + O_2(X,^3\Sigma_g^-) + M \xrightarrow{k_{34}} ClO_2(\tilde{X},^2B_1) + M \quad (35)$$

For these two reactions, it is reasonable to assume that there is a negligible contribution of the Chaperon mechanism to the reaction process.[67] The parameters needed to calculate k_{34} and k_{35} are presented in Table 4. The deactivation rate constants obtained using the newly developed model are presented in Table 5 together with the rate constants recommended by IUPAC.[46] The recommendations from IUPAC are based on data from laboratory experiments. Table 5 shows that the theoretically calculated results are only a factor of 1.83−8.34 lower than those obtained from experiments, and all the theoretical rates are lower than those obtained experimentally. The estimation of the rate constant of termolecular reactions using statistical or empirical-adapted methods is not an easy task. The main problem is related to the calculation of the reaction probability for deactivation of the quasi-bound molecule, p_{deac}. There is clear evidence that the termolecular rate constant will be highly overestimated if the assumption $p_{deac} = 1$ is used.[65−67] Therefore, considering the simplicity of the semiempirical model described in this paper, underestimations of the rate constants by factors of only 1.83−8.34 compared with experimental data for the reactions 34 and 35 are good results.

TABLE 5: Termolecular Rate Constant, k_{ter}, for Formation of O_3 and ClO_2, and Relative Derivation between the Theoretical and Experimental Rate Constants[a]

$O(^3P) + O_2(X,^3\Sigma_g^-) + M \rightarrow O_3(\tilde{X},^1A_1) + M$

	$M = O_2(X,^3\Sigma_g^-)$			$M = N_2(X,^1\Sigma_g^+)$		
T, K	$k_{ter}^{a=0}$	$k_{ter}^{a=0.2}$	k_{ter}^{exp}	$k_{ter}^{a=0}$	$k_{ter}^{a=0.2}$	k_{ter}^{exp}
200	17.16	10.55	18.67	28.77	1.769	17.43
300	4.644	4.644	6.000	7.785	7.785	5.600
derivation	0.1608	0.3293		0.5072	0.2046	

$Cl(^2P) + O_2(X,^3\Sigma_g^-) + M \rightarrow ClO_2(\tilde{X},^2B_1) + M$

	$M = O_2(X,^3\Sigma_g^-)$			$M = N_2(X,^1\Sigma_g^+)$		
T, K	$k_{ter}^{a=0}$	$k_{ter}^{a=0.1}$	k_{ter}^{exp}	$k_{ter}^{a=0}$	$k_{ter}^{a=-0.9}$	k_{ter}^{exp}
200	29.34	18.78	51.85	49.44	47.47	68.06
300	8.694	8.694	16.00	14.65	14.65	14.00
derivation	0.4462	0.5472		0.1198	0.1346	

[a] The rate constants are calculated based on the model developed in this study. k_{ter}^{exp}: the recommendations from IUPAC.[46] The units for all the rate constants are 10^{-34} cm^6 $molecule^{-1}$ s^{-1}. The derivations are calculated from the theoretically calculated rates and the recommendations from IUPAC as follows: derivation $= (\sum|k_{ter}^{theo} - k_{ter}^{exp}|)/k_{ter}^{exp}N_{tot}$. N_{tot} is the number of rate constants included in the summation (here 101).

Using the potential energy information and the spectroscopic data from the DFT calculation on the DMSOH + O_2 → DMS(OH)(OO) system, and the Lennard-Jones parameters plus the $\langle\Delta E_{trans}\rangle$ values for $O_2(X,^3\Sigma_g^-)$ and $N_2(X,^1\Sigma_g^+)$ given in Table 4, we have calculated k'_{5b} for $a = 0$ and 0.8 (the value 0.8 was chosen since we assume that reaction 5b has the same temperature dependence as $C_2H_5 + O_2 + M \rightarrow C_2H_5O_2 + M$). Figure 6 presents the results obtained for k_{5b} for $M = O_2$ and N_2. Since we found that $k'^{a=0}_{5b} \approx k'^{a=0.8}_{5b}$ only the results for $k'^{a=0}_{5b}$ are presented in the paper.

4. Results and Discussions of the Estimated Rate Constants for Reaction 5

4.1. Experiments. Compared with the reaction between DMS and OH, reaction 5 has not been intensively studied, however experimental studies of the isotopic variance of the reaction DMSOH + O_2 → have been presented in three papers: Hynes et al.,[33,38] and Barone et al.[24]

The determination of the rate constant for reaction 4 using experimental methods are based on an indirect rate determination and measured rate constant along with measured rate constants of reactions 1 (k_1) and 2 (k_2, k_{-2}). Therefore, uncertainties in the determination of k_1, k_2, and k_{-2} influence the determination of k_4. Hynes et al.[33] used two different experimental setups to investigate these three reactions. The first experimental setup was a conventional flash photolysis−resonance fluorescence

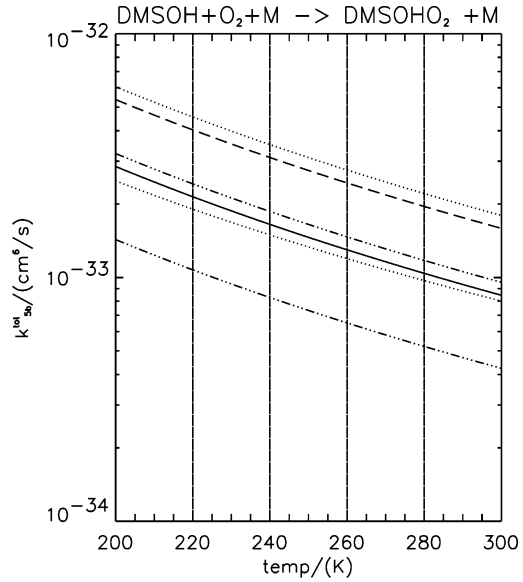

Figure 6. Calculated rate constants and estimated errors for reaction 5b as a function of temperature. k_{5b}^{tot} for M = O_2 (solid line), its corresponding errors are the dashed−dotted lines. k_{5b}^{tot} for M = N_2 (dashed line), its corresponding errors are the dotted lines. The rate constants are estimated using the theoretical model described in section 3.2. The errors are estimated from the assumption that the relative energies displayed in Table 3 have a possible error of 10%, and the distance between the center of masses of DMSOH and O_2 at equilibrium can be 0.4 Å lower.

(FP−RF) apparatus. The second setup was a pulsed-laser photolysis−pulsed-laser-induced fluorescence (PLP−PLIF) apparatus. The PLP−PLIF apparatus was developed in order to examine OH−sulfide reactions under conditions close to those prevailing in the atmosphere. From these experiments the rate constant of reaction 4 was measured at 261 K and a total pressure of 700 Torr using two different bath gases: O_2 and atmospheric air.

Hynes et al.[38] investigated reaction 4 using a PLP−PLIF apparatus at two different temperatures (250 and 258 K) at a total pressure of 110 Torr using two different bath gases: He and N_2.

The most extensive experimental study of Reaction 4 has been done by Barone et al.[24] who used the PLP−PLIF technique to measure the rate constant at eight different temperatures from 222 to 258 K and five different pressures from 30 to 200 Torr using two different bath gases: He and N_2.

In Table 6, we have collected all the results from these three experimental studies. Because this isotopic reaction only corresponds to secondary isotope effects the results obtained by these groups can be compared with the theoretically estimated results in this paper. The experiments from the three groups showed that the rate constants were almost temperature and pressure independent; however, only one of the experiments was performed under conditions typical of the atmospheric boundary layer; temperatures (≈260−298 K) and pressure (1 atm).

In Table 6 we observe that the work by Hynes et al.[33] gives a result which is factors of 3.1 to 6.5 higher than those obtained by Barone et al.[24] and Hynes et al.[38] However, a reanalysis of the rate constants obtained from the study by Hynes et al.,[33] using the equilibrium constant k_2/k_{-2} from the Hynes et al.[38] study to adjust the rate constant from Hynes et al.[33] presented in Table 6, gave rate constants which were in good agreement with the other experimental rate constants presented in Table 6.[38] However, Hynes et al.[38] did not present the adjusted rates in their paper.

TABLE 6: k_{5a} and k_{5b} Rate Constants Compared with the Experimentally Obtained Rate Constant for the Total Reaction between DMSOH and O_2

			k, 10^{-13} cm^3 molecule^{-1} s^{-1}						
			k_{5a}^{theo}		k_{5b}^{theo}				
T, K	p, Torr	bath gas	av	low	av	low	high	k_5^{exp}	ref
222	100	He	91.8	15.3				(8.9 ± 1.4)	24
228	100	N_2	76.4	13.4	0.259	0.130	0.292	(8.5 ± 2.7)	24
228	100	N_2	76.4	13.4	0.259	0.130	0.292	(9.1 ± 0.6)	24
229	100	He	74.2	13.1				(7.8 ± 3.6)	24
230	30	N_2	72.1	12.8	0.249	0.125	0.281	(8.6 ± 1.6)	24
230	100	He	72.1	12.8				(8.8 ± 0.9)	24
233	75	N_2	66.2	12.0	0.176	0.0885	0.199	(11.8 ± 3.0)	24
233	80	N_2	66.2	12.0	0.187	0.0944	0.212	(11.5 ± 2.6)	24
234	100	He	64.4	11.8				(10.5 ± 2.2)	24
234	100	He	64.4	11.8				(8.4 ± 2.4)	24
247	100	N_2	45.9	9.18	0.180	0.0906	0.203	(10.9 ± 0.7)	24
247	100	N_2	45.9	9.18	0.180	0.0906	0.203	(10.9 ± 0.5)	24
250	110	He	42.7	8.71				(8.0 ± 0.3)	38
250	110	N_2	42.7	8.71	0.188	0.0945	0.212	(6.5 ± 0.3)	38
258	100	N_2	35.7	7.64	0.148	0.0746	0.168	(10.1 ± 0.5)	24
258	200	N_2	35.7	7.64	0.297	0.149	0.335	(9.9 ± 0.3)	24
258	100	N_2	35.7	7.64	0.148	0.0746	0.168	(13.7 ± 2.7)	24
258	110	N_2	35.7	7.64	0.163	0.0821	0.184	(6.5 ± 0.3)	38
258	110	He	35.7	7.64				(7.0 ± 0.3)	38
258	110	N_2	35.7	7.64	0.163	0.0821	0.184	(8.4 ± 0.3)	38
261	700	O_2	33.5	7.29	0.539	0.270	0.609	(42 ± 22)	33
261	700	air	33.5	7.29	0.919	0.462	1.04	(42 ± 22)	33

[a] For k_{5a}, av is the theoretical determined rate constant, and low is the lower limit of the theoretical determined rate constant. For k_{5b}, av is the theoretically determined rate constant, low is the lower limit of the theoretically determined rate constant, and high is the higher limit of the theoretically determined rate constant.

Barone et al.[24] observed that the rate constant of reaction 5 did not depend on the concentration of DMS and O_2 or the isotopic variant of DMS and O_2. They concluded that this invariance suggested that the methyl groups in the DMSOH adduct are not directly involved in reaction 5. This observation is substantiated by the CPES shown in Figure 4 and the obtained reaction path for reaction 5a. Furthermore, if reaction 5c takes place it is natural that it occurs through the following intermediate complex (†):

$$O_2 + CH_3S(OH)CH_3 \rightarrow [OO - CH_3S(OH)CH_3]^{\dagger}$$

$$[OO - CH_3S(OH)CH_3]^{\dagger} \rightarrow CH_3O_2 + CH_3S(OH) \qquad (36)$$

The observation from Barone et al.[24] indicates that if reaction sequence 37 is correct, it will not take place. Some studies (e.g., Gross and Baklanov,[12] Yin et al.,[13] Barone et al.,[24] and Turnipseed[59]) have included reactions where the bond between sulfur and carbon in DMSOH breaks without any interaction with other chemical compounds. A comparison of the PW91PW91 results of DMSOH (Figure 2) and DMS(OH)(OO) (Figure 3) shows that O_2 stabilizes the bond between the sulfur atom in DMS and the oxygen atom in OH (compare the distances shown in Table 1 with r_{S-OH} in Table 2). The reason for this stabilization is primarily related to electrostatic interactions between O_2 and the electron cloud centered at the sulfur atom. Therefore, if O_2 reacts with DMSOH, as proposed in reaction 37, this reaction will have a higher probability to occur than a sulfur carbon bond cleavage in DMSOH without any interactions with O_2. The observations from Barone et al.[24] and this study indicate that these processes do not occur under typical atmospheric conditions.

Hynes et al.[33] measured the same rate constant for reaction 5 at $T = 261$ K and $p_{O_2} = p_{air} = 700$ Torr. This result shows that, if the termolecular reaction 5b is important, then the Charperon mechanism can be neglected, since as explained in section 2.2.2, it is reasonable to assume that for $M = O_2$ only the exchange-energy transfer mechanism is active, and for M = air 80% of M is N_2.

4.2. Theoretical Derivations. In the previous section, it was mentioned that the experimental determination of k_5 depends on an indirectly measured rate constant and the measured values for k_1, k_2, and k_{-2}. This is not the case for the theoretically calculated rate constants. Using theoretical methods to calculate rate constants the information and quality from PES/CPES and spectroscopic data are crucial. We have used PW91PW91/6-311G** to calculate potential energies and spectroscopic data of the reactants and products in reactions 5a and 5b, and used these data to estimate the rate constants k_{5a} and k_{5b}^{tot} of these two reactions from 200 to 300 K. This temperature interval was chosen since typical atmospheric boundary layer, and free tropospheric and stratospheric temperatures are in this temperature interval.[76] The calculated rate constants are presented in Figures 5 and 6.

Sections 2.2.1 and 2.2.2 showed that k_{5a} and k_{5b}^{tot} are pressure independent. On the other hand, if we want to evaluate the atmospheric importance of reactions 5a and 5b we must calculate k_{5b}:

$$k_{5b} = [M] \times k_{5b}^{tot} \qquad (37)$$

i.e. k_{5b} is pressure dependent. To compare the results obtained in this study with the rate constants obtained by the experiments, we have calculated the rate constants for the different temperatures, pressures and bath gases of N_2, O_2 and air used in the experiments and listed in Table 6 together with the experimentally obtained rate constants. We observe that the theoretical results obtained for $k_{5a} + k_{5b}$ (correspond to $k_{5a}^{av} + k_{5b}^{av}$ in Table 6) are approximately factors of 2.61 to 10.3 higher than the experimental results from Hynes el at.[38] and Barone et al.,[24] while the experimental results from Hynes et al.[33] are factors of 0.81 and 0.87 smaller than the results obtained in this study. Considering the simplicity of the theoretical models described in sections 3.1 and 3.2 and the method used to calculate the necessary potential energies and spectroscopic data, the agreement between theory and experiment is reasonably good. If we compare the experimental results with rate constants at the lower error bar in Table 6 ($k_{5a}^{low} + k_{5b}^{low}$), the agreement between experiment and theory is excellent.

Well-known differences between DFT and ab initio methods compared to the correct equilibrium structure for molecules exist.[78,79] These differences in bond lengths, angles and vibrational frequencies will decrease the rate constants calculated in this paper; i.e., the agreement between the results from Hynes et al.[38] and Barone et al.[24] then would be improved.

To understand the atmospheric importance of the two reaction channels 5a and 5b, we have plotted in Figure 7 the theoretically calculated rate constant for k_{5a}, k_{5b} at 1 atm air and the sum of these two rate constants as a function of the temperature together with the experimentally obtained rate constants. Figure 7 shows that the temperature dependence of k_5 predicted by this study disagrees with the results obtained by Hynes et al.[38] and Barone et al.[24]; their results showed a temperature independence. However, in the two experimental studies rate constants were only measured over the temperature range from 222 to 258 K, and in this temperature interval we obtain a very small negative temperature dependence. For reactions 5a and 5b with $M = O_2$ and reaction 5b with $M = N_2$, the rate constants decrease by factors of 2.57, 1.58, and 1.57 in the temperature range from 222 to 258 K, respectively.

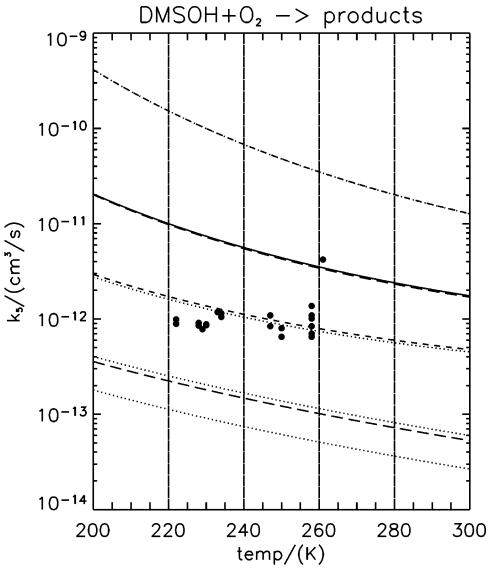

Figure 7. Calculated rate constants for reactions 5a and 5b, and the sum of these two rate constants as a function of temperature. Upper long dashed line: k_{5a}. Corresponding errors: upper dotted lines. Lower long dashed line: k_{5b}. Corresponding errors: lower dotted lines. Solid line: $k_{5a} + k_{5b}$. Corresponding errors: small dashed lines. The dots are the experimentally measured rate constants displayed in Table 6. The rate constants are estimated using the theoretical models described in sections 3.1 and 3.2. The errors are estimated from the assumptions described in the captions for Figures 5 and 6. [M] is equal to 1 atm of air.

The model used to calculate k_5 considers reaction 5a to be a two step mechanism. Even though step two in this proposed mechanism is the rate determining step, e.g., step one could perhaps be ignored in the calculation of the overall rate constant, Table 3 shows that the rate dependence will change from a negative to a positive temperature dependence if step one is ignored.

The studies by Hynes et al.[33,38] and Barone et al.[24] did not investigate the branching ratio of reaction 5, but two experimental mechanistic studies[59,77] have reported possible branching ratios of reaction 5. Turnipseed et al.[59] reported a branching ratio of 0.50 ± 0.15 for channel 5a and for the rest of the channels in reaction 5 0.50 ± 0.15. Arsene et al.[77] reported that the major product channel of reaction 5 under NO_x free conditions is channel 5a. Arsene et al.[77] wrote that the reason for this discrepancy was not completely clear, but it could be related to the reaction conditions employed in the two studies, since Turnipseed et al.[59] used NO to convert HO_2 to OH for determining the branching ratio of channel a, i.e., not a NO_x free study. Later Arsene et al.[47] have shown that the NO_x conditions employed in the experiments influences the formation of DMSO. Table 6 and Figure 7 substantiate the results from Arsene et al.,[77] i.e., channel 5a is the dominant product channel of reaction 5.

Figure 7 shows that channel 5b has very little influence on the total rate constant for reaction 5. However, in the theoretical methods used to calculate the rate constants for reactions 5a and 5b two parameters are especially sensitive: (1) $\Delta E_{tot}^{5a} = \Delta E_{11} + V_0(\#)$ of channel 5a and (2) the proposed averaged energy transfer which M obtains when it collides with the highly excited molecule ($\langle \Delta E_{trans} \rangle$) in channel 5b.

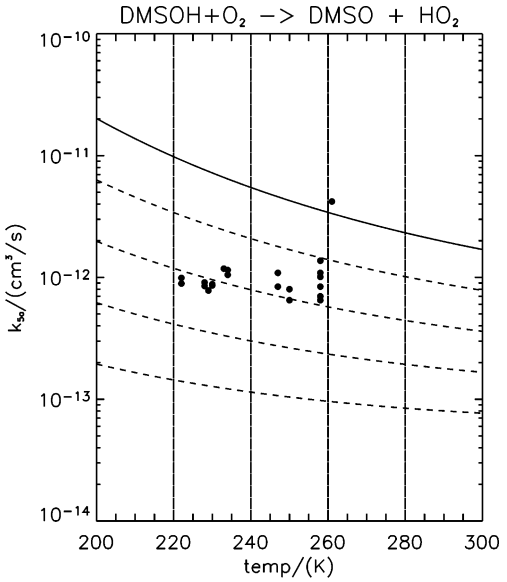

Figure 8. Sensitivity study of the influence of ΔE_{tot}^{5a} on k_{5a} as a function of the temperature. Solid line: calculated k_{5a} with $\Delta E_{tot}^{5a} = \Delta E_{11} + V_0(\#)$. Dashed lines: calculated k_{5a} with $\Delta E_{tot}^{5a} = \Delta E_{11} + V_0(\#) - 0.02$ eV (upper curve) to $\Delta E_{tot}^{5a} = \Delta E_{11} + V_0(\#) - 0.08$ eV (lowest curve). The dots are the experimentally measured rate constants displayed in Table 6. The rate constants are estimated using the theoretical model described in section 3.1.

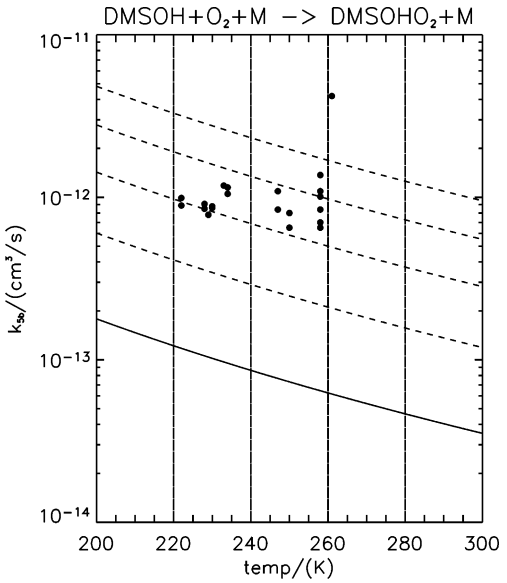

Figure 9. Sensitivity study of the influence $\langle \Delta E_{trans} \rangle$ on k_{5b} ([M] equal to 1 atm of air) as a function of temperature. Solid line: k_{5b} as in Figure 7. Dashed lines: $k_{5b} \times$ [M] with an increase of $\langle \Delta E_{trans} \rangle$ by 50% (lowest curve) to an increase of $\langle \Delta E_{trans} \rangle$ 200% (upper curve).

To demonstrate the sensitivity of ΔE_{tot}^{5a}, k_{5a} has been recalculated after ΔE_{tot}^{5a} has been lowered by 0.02, 0.04, 0.06, and 0.08 eV. The result from this sensitivity study is shown in Figure 8. Besides a very drastic decrease in k_{5a} when ΔE^{5a} is lowered by only 0.08 eV (at 300 K, k_{5a} decreases by a factor of 22.1 and at 200 K by a factor of 103.7), k_{5a} became almost temperature independent.

Figure 9 shows the results from a sensitivity study of k_{5b} relative to $\langle \Delta E_{trans} \rangle$. In this study the average energy transfer for M equal to O_2 or N_2 have been increased by 50%, 100%, 150% and 200% and recalculations of k_{5b} have been performed. The increase of $\langle \Delta E_{trans} \rangle$ by 200% corresponds to a $\langle \Delta E_{trans} \rangle$ value which is a little smaller than that obtained for H_2O when it collides with toluene.[75] We observe that the temperature dependence of k_{5b} does not change when $\langle \Delta E_{trans} \rangle$ is increased, and an increase of 100% of $\langle \Delta E_{trans} \rangle$ brings k_{5a} in the range of the experimentally measured rate constants from Hynes et al.[38] and Barone et al.[24]

5. Conclusion

Many uncertainties still relate to the chemical fate of DMS in the marine boundary layer, and therefore also the addition path of DMS + OH illustrated in Figure 1; these uncertainties are related to both reaction paths and rate constants. The fate of DMSOH in the atmosphere will be its reaction with O_2 due to the high atmospheric concentrations of O_2. The results from the work presented here support the point that channel 5a is by far the most dominant channel in reaction 5, and it is not very likely that channel 5c occurs under typical atmospheric conditions.

It was concluded in the work by Hynes et al.[38] and Barone et al.[24] that the total rate constant (k_5) for reaction 5 was pressure independent. Since only reaction channel 5b in reaction 5 is pressure dependent, a further conclusion from these studies must be that channel 5b is insignificant under atmospheric conditions. That is, k_{5b}^{tot} in eq 37 is very small. On the basis of the results from this study, the high sensitivity in the theoretical models used to calculate k_{5a} and k_{5b}, and the test of the semiempirical model on O + O_2 + M and Cl + O_2 + M which gave results which were factors of 1.83−8.34 lower than the experiments, we also conclude that it is possible that channel 5b can contribute up to 50% at the most.

This paper presents the first theoretical study where the interaction between DMSOH + $O_2(^3\Sigma_g)$ has been investigated using DFT and ab initio methods combined with theoretical rate constant calculations. Even though higher order ab initio methods and larger basis sets would have enhanced the agreement between the theoretically calculated rate constant (presented in the paper) and the experimentally measured rates this is not an easy task to do. In any event, the results from this study indicate that experimental measurements of the rate constant k_5 should be performed over a broader temperature and pressure range, and reaction molecular dynamics studies should be made.

Acknowledgment. This research was supported by the European Commission as a part of the fifth Framework Program project "Evaluation of the Climate Impact of Dimethyl Sulfide (EL CID)" [I.B., A.G.], the Danish Center for Scientific Computing [A.G., R.M.S, J.K, K.V.M.], the AFO2000 Atmospheric Research Program within the project REHATROP [I.B.], Statens Naturvidenskabelige Forskningsråd [K.V.M.], Statens Teknisk Videnskabelige Forskningsråd [K.V.M], and EU network MOLPROP+THEONETII [K.V.M].

Note Added after ASAP Posting. Several values in Table 6 were inadvertently shifted from the original submission. This paper was posted ASAP on 7/21/04. The corrected version was reposted on 8/10/04.

References and Notes

(1) Dingenen, R. Van; Jensen, N. R.; Hjorth, J.; Raes, F. *J. Atmos. Chem.* **1994**, *18*, 211.

(2) Andrea, M. O. *Marine Chem.* **1990**, *30*, 1.

(3) Bates, T. S.; Cline, J. D.; Gammon, R. H.; Kelly-Hansen, S. R. *J. Geophys. Res.* **1987**, *92*, 2930.

(4) Spiro, P. A.; Jacob, D. J.; Logan, J. A. *J. Geophys. Res.* **1992**, *97*, 6023.

(5) Bates, T. S.; Lamb, B. K.; Guenther, A.; Dignon, J.; Stoiber, R. E. *J. Atmos. Chem.* **1992**, *14*, 315.
(6) Berresheim, H.; Wine, P. H.; Davis, D. D. *Sulphur in the Atmosphere, in Composition, Chemistry and Climate of the Atmosphere*; Singh, H. B., Ed.; Van Nostrand Reinhold: New York, 1995; p 251.
(7) Charlson, R. J.; Lovelock, J. E.; Andrea, M. O.; Warren, S. G. *Nature* **1987**, *326*, 655.
(8) Pandis, S. N.; Russel, L. M.; Seinfeld, J. H. *J. Geophys. Res.* **1994**, *99*, 16945.
(9) Russel, L. M.; Pandis, S. N.; Seinfeld, J. H. *J. Geophys. Res.* **1994**, *99*, 20989.
(10) Pirjola, L.; O'Dowd, C. D.; Brooks, I. M.; M. Kulmala, M. *J. Geophys. Res.* **2000**, *105*, 26531.
(11) Yoon, Y. J.; Brimblecombe, P. *Atmos. Chem. Phys.* **2002**, *2*, 17.
(12) Gross, A.; Baklanov, A. *Int. J. Environ. Pollution* **2004**, in press.
(13) Yin, F.; Grosjean, D.; Seinfeld, J. H. *J. Atmos. Chem.* **1990**, *11*, 309.
(14) Yin, F.; Grosjean, D.; Flagan, F. C.; Seinfeld, J. H. *J. Atmos. Chem.* **1990**, *11*, 365.
(15) Koga, S.; Tanaka, H. *J. Atmos. Chem.* **1993**, *17*, 201.
(16) Capaldo, K. P.; Pandis, S. N. *J. Geophys. Res.* **1997**, *102*, 23251.
(17) Campolongo, F.; Saltelli, A.; Jensen, N. R.; Wilson, J.; Hjorth, J. *J. Atmos. Chem.* **1999**, *32*, 327.
(18) Barone, S. B.; Turnipseed, A. A.; Ravishankara, A. R. *Faraday Discuss.* **1995**, *100*, 39.
(19) Wilson, C.; Hirst, D. M. *Prog. React. Kinet.* **1996**, *21*, 68.
(20) Ravishankara, A. R.; Rudich, Y.; Talukdar, R.; Barone, S. B. *Philos. Trans. R. Soc. London B.* **1997**, *352*, 171.
(21) Urbanski, S. P.; Wine, P. H. *S−Centered Radicals*; Alfassi, Z., Ed.; John Wiley & Sons: New York, **1999**; p 97.
(22) EL CID. "Final report of the EC 5FP project: Evaluation of the Climate Impact of Dimethyl Sulphid (ELCID). Project coordinator Prof. I. Barnes. Contract number: EVK2−CT-1999−00033". 2003.
(23) Glasow, R. von; Crutzen, P. J. *Atmos. Chem. Phys. Discuss.* **2003**, *2*, 6733.
(24) Barone, S. B.; Turnipseed, A. A.; Ravishankara, A. R. *J. Phys. Chem.* **1996**, *100*, 14694.
(25) Atkinson, R.; Perry, R. A.; Pitts, J. N., Jr. *Chem. Phys. Lett.* **1978**, *54*, 14.
(26) Kurylo, M. J. *Chem. Phys. Lett.* **1978**, *58*, 233.
(27) Cox, R.; Sheppard, D. *Nature (London)* **1980**, *284*, 330.
(28) Wine, P. H.; Kreutter, N. M.; Gump, C. A.; Ravishankara, A. R. *J. Phys. Chem.* **1981**, *85*, 2660.
(29) Macleod, H.; Poulet, G.; LeBras, G. *J. Chim. Phys.* **1983**, *80*, 287.
(30) Atkinson, R.; Pitts, J. N., Jr.; Aschmann, S. M. *J. Phys. Chem.* **1984**, *88*, 1584.
(31) Martin, D.; Jourdan, J. L.; LeBras, G. *Int. J. Chem. Kinet.* **1985**, *17*, 1247.
(32) Wallington, T. J.; Atkinson, R.; Tuazon, E. C.; Aschmann, S. M. *Int. J. Chem. Kinet.* **1986**, *18*, 837.
(33) Hynes, A. J.; Wine, P. H.; Semmes, D. H. *J. Phys. Chem.* **1986**, *90*, 4148.
(34) Hsu, Y.-C.; Chen, D.-S.; Lee, Y.-P. *Int. J. Chem. Kinet.* **1987**, *19*, 1073.
(35) Barnes, I.; Bastian, V.; Becker, K. H. *Int. J. Chem. Kinet.* **1988**, *20*, 415.
(36) Nielsen, O. J.; Sidebottom, H. W.; Nelson, L.; Treacy, J. J.; O'Farrell, D. J. *Int. J. Chem. Kinet.* **1989**, *21*, 1101.
(37) Abbatt, J. P. D.; Fentner, F. F.; Anderson, J. G. *J. Phys. Chem.* **1992**, *96*, 1780.
(38) Hynes, A. J.; Stocker, R. B.; Pounds, A. J.; McKay, T.; Bradshaw, J. D.; Nicovich, J. M.; Wine, P. H. *J. Phys. Chem.* **1995**, *99*, 16967.
(39) Williams, M. B.; Campuzano-Jost, P.; Bauer, D.; Hynes, A. J. *Chem. Phys. Lett.* **2001**, *344*, 61.
(40) McKee, M. L. *J. Phys. Chem.* **1993**, *98*, 10971.
(41) Gu, M.; Turecek, F. *J. Am. Chem.* **1992**, *114*, 7146.
(42) Turecek, F. *J. Phys. Chem.* **1994**, *98*, 3701.
(43) Turecek, F. *Collect. Czech. Chem. Commun.* **2000**, *65*, 455.
(44) Wang, L.; Zhang, J. *J. Mol. Struct. (THEOCHEM)* **2001**, *543*, 167.
(45) Sander, S. P.; Friedl, R. R.; DeMore, W. B.; Golden, D. M.; Kurylo, M. J.; Hampson, R. F.; Hoie, R. E.; Moortgat, G. K.; Ravishankara, A. R.; Kolb, C. E.; Molina, M. J. *JPL Publ. 00-3* **2000**, *3*, 1.
(46) Atkinson, R.; Baulch, D. L.; Cox, R. A.; Crowley, J. N.; Hampson, R. F.; Hynes, R. G.; Jenkin, M. E.; Rossi, M. J.; Troe, *J. Atmos. Chem. Phys. Discuss.* **2003**, *3*, 6179.
(47) Arsene, C.; Barnes, I.; Becker, K. H.; Mocanu, R. *Atmos. Environ.* **2001**, *35*, 3769.
(48) Jensen, F. *Introduction to Computational Chemistry*; John Wiley & Sons: New York, 1998.
(49) Frisch, M. J.; Trucks, G. W.; Schlegel, H. B.; Scuseria, G. E.; Robb, M. A.; Cheeseman, J. R.; Zakrzewski, V. G.; Montgomery, J. A.; Stratmann, R. E.; Burant, J. C.; Dapprich, S.; Millam, J. M.; Daniels, A. D.; Kudin, K. N.; Strain, M. C.; Farkas, O.; Tomasi, J.; Barone, V.; Cossi, M.; Cammi, R.; Mennucci, B.; Pomelli, C.; Adamo, C.; Clifford, S.; Ochterski, J.; Petersson, G. A.; Ayala, P. Y.; Cui, Q.; Morokuma, K.; Malick, D. K.; Rabuck, A. D.; Raghavachari, K.; Foresman, J. B.; Cioslowski, J.; Ortiz, J. V.; Stefanov, B. B.; Liu, G.; Liashenko, A.; Piskorz, P.; Komaromi, I.; Gomperts, R.; Martin, R. L.; Fox, D. J.; Keith, T.; Al-Laham, M. A.; Peng, C. Y.; Namayakkara, A.; Gonzalez, C.; Challacombe, M.; Gill, P. M. W.; Johnson, B. G.; Chen, W.; Wong, M. W.; Andres, J. L.; Head-Gordon, M.; Replogle, E. S.; Pople. J. A. *Gaussian 98 (Revision A.6 and, A.7)*; Gaussian Inc., Pittsburgh, PA, 1998.
(50) Lee, C.; Yang, W.; Parr, R. G. *Phys. Rev. B*, **1988**, *37*, 785.
(51) Becke, J. *J. Chem. Phys.* **1997**, *107*, 8554.
(52) Perdew, J. P.; Wang, Y. *Phys. Rev. B* **1992**, *45*, 13244.
(53) Perdew, J. P.; Burke, K.; Wang, T. *Phys. Rev. B* **1996**, *54*, 16533.
(54) Møller, C.; Plesset, M. S. *Phys. Rev.* **1934**, *46*, 618.
(55) Krishnan, R.; Blinkley, J. S.; Seeger, R.; Pople, J. A. *J. Chem. Phys.* **1980**, *72*, 650.
(56) Dunning, T. H., Jr. *J. Chem. Phys.* **1989**, *90*, 1007.
(57) Wilson, A. K.; van Mourik, T.; Dunning T. H., Jr. *J. Mol. Struct.* **1996**, *388*, 339.
(58) Kendall, R. A.; Dunning, T. H., Jr.; Harrison, R. J. *J. Chem. Phys.* **1992**, *103*, 4572.
(59) Turnipseed, A. A.; Barone, S. B.; Ravishankara, A. R. *J. Phys. Chem.* **1996**, *100*, 14703.
(60) Keck, J. *J. Chem. Phys.* **158**, *29*, 410.
(61) Bunker, D. L.; Davidson, N. *J. Am. Chem. Soc.* **1958**, *80*, 5090.
(62) Bunker, D. L. *J. Chem. Phys.* **1960**, *32*, 1001.
(63) Roberts, R. E.; Bernstein, R. B.; Curtiss, C. F. *J. Chem. Phys.* **1969**, *50*, 5163.
(64) Whitlock, P. A.; Mucherman, J. T.; Roberts, R. E. *J. Chem. Phys.* **1974**, *600*, 3658.
(65) Gross, A.; Billing, G. D. *Chem. Phys.* **1993**, *173*, 393.
(66) Gross, A.; Billing, G. D. *Chem. Phys.* **1994**, *187*, 329.
(67) Gross, A.; Billing, G. D. *Chem. Phys.* **1997**, *217*, 1.
(68) Billing, G. D.; Mikkelsen, K. V. *Introduction to Molecular Dynamics and Chemical Kinetics*; John Wiley & Sons: New York, 1996.
(69) Gilbert, R. G.; Smith, S. C. *Theory of Unimolecular and Recombination Reactions*; Blackwell Scientific Publications: Oxford, England, 1990.
(70) Gallucci, C. R.; Schatz, G. C. *J. Phys. Chem.* **1982**, *86*, 2352.
(71) Blint, R. J. *J. Chem. Phys.* **1980**, *73*, 765.
(72) Herzberg, G. *Molecular Spectra and Molecular Structure: III. Electronic spectra and Electronic Structure of Polyatomic Molecules*; D. van Nostrand Company Inc., New York, 1966.
(73) Peterson, K. A.; Werner, H.-J. *J. Chem. Phys.* **1992**, *96*, 8948.
(74) Cuadros, F.; Cachadiña, I.; Ahamuda, W. *Mol. Eng.* **1996**, *6*, 319.
(75) Hippler, H.; Troe, J.; Wendelken, H. J. *J. Chem. Phys.* **1983**, *78*, 6709.
(76) Jacobson, M. Z. *Fundamentals of Atmospheric Modeling*; Cambridge University Press: Cambridge, U.K. 1999.
(77) Arsene, C.; Barnes, I.; Becher, K. H. *Phys. Chem. Chem. Phys.* **1999**, *1*, 5463.
(78) Gross, A.; Stockwell, W. R.; Mikkelsen, K. V. *Int. J. Quantum Chem.* **2001**, *84*, 479.
(79) Gross, A.; Stockwell, W. R.; Mikkelsen, K. V. *Int. J. Quantum Chem.* **2001**, *84*, 493.